

Dear Author,

Here are the proofs of your article.

- You can submit your corrections **online**, via **e-mail** or by **fax**.
- For **online** submission please insert your corrections in the online correction form. Always indicate the line number to which the correction refers.
- You can also insert your corrections in the proof PDF and **email** the annotated PDF.
- For fax submission, please ensure that your corrections are clearly legible. Use a fine black pen and write the correction in the margin, not too close to the edge of the page.
- Remember to note the **journal title**, **article number**, and **your name** when sending your response via e-mail or fax.
- **Check** the metadata sheet to make sure that the header information, especially author names and the corresponding affiliations are correctly shown.
- **Check** the questions that may have arisen during copy editing and insert your answers/ corrections.
- **Check** that the text is complete and that all figures, tables and their legends are included. Also check the accuracy of special characters, equations, and electronic supplementary material if applicable. If necessary refer to the *Edited manuscript*.
- The publication of inaccurate data such as dosages and units can have serious consequences. Please take particular care that all such details are correct.
- Please **do not** make changes that involve only matters of style. We have generally introduced forms that follow the journal's style. Substantial changes in content, e.g., new results, corrected values, title and authorship are not allowed without the approval of the responsible editor. In such a case, please contact the Editorial Office and return his/her consent together with the proof.
- If we do not receive your corrections **within 48 hours**, we will send you a reminder.
- Your article will be published **Online First** approximately one week after receipt of your corrected proofs. This is the **official first publication** citable with the DOI. **Further changes are, therefore, not possible.**
- The **printed version** will follow in a forthcoming issue.

Please note

After online publication, subscribers (personal/institutional) to this journal will have access to the complete article via the DOI using the URL: [http://dx.doi.org/\[DOI\]](http://dx.doi.org/[DOI]).

If you would like to know when your article has been published online, take advantage of our free alert service. For registration and further information go to: <http://www.springerlink.com>.

Due to the electronic nature of the procedure, the manuscript and the original figures will only be returned to you on special request. When you return your corrections, please inform us if you would like to have these documents returned.

Metadata of the article that will be visualized in OnlineFirst

Please note: Images will appear in color online but will be printed in black and white.

ArticleTitle	Probing the Combined Effect of Flunitrazepam and Lidocaine on the Stability and Organization of Bilayer Lipid Membranes. A Differential Scanning Calorimetry and Dynamic Light Scattering Study	
Article Sub-Title		
Article CopyRight	Springer Science+Business Media New York (This will be the copyright line in the final PDF)	
Journal Name	Cell Biochemistry and Biophysics	
Corresponding Author	Family Name	Perillo
	Particle	
	Given Name	María A.
	Suffix	
	Division	Cátedra de Química Biológica, Departamento de Química, FCEyN
	Organization	Instituto de Investigaciones Biológicas y Tecnológicas (IIBYT), CONICET-Universidad Nacional de Córdoba
	Address	Av. Vélez Sarsfield 1611, X5016GCA, Córdoba, Argentina
	Email	mperillo@efn.uncor.edu
Author	Family Name	Caruso
	Particle	
	Given Name	Benjamín
	Suffix	
	Division	Cátedra de Química Biológica, Departamento de Química, FCEyN
	Organization	Instituto de Investigaciones Biológicas y Tecnológicas (IIBYT), CONICET-Universidad Nacional de Córdoba
	Address	Av. Vélez Sarsfield 1611, X5016GCA, Córdoba, Argentina
	Email	bcaruso@efn.uncor.edu
Author	Family Name	Sánchez
	Particle	
	Given Name	Julieta M.
	Suffix	
	Division	Cátedra de Química Biológica, Departamento de Química, FCEyN
	Organization	Instituto de Investigaciones Biológicas y Tecnológicas (IIBYT), CONICET-Universidad Nacional de Córdoba
	Address	Av. Vélez Sarsfield 1611, X5016GCA, Córdoba, Argentina
	Email	jmsanchez@efn.uncor.edu
Author	Family Name	García
	Particle	
	Given Name	Daniel A.
	Suffix	
	Division	Cátedra de Química Biológica, Departamento de Química, FCEyN
	Organization	Instituto de Investigaciones Biológicas y Tecnológicas (IIBYT), CONICET-Universidad Nacional de Córdoba
	Address	Av. Vélez Sarsfield 1611, X5016GCA, Córdoba, Argentina
	Email	dagarcia@efn.uncor.edu

Author	Family Name	Paula
	Particle	de
	Given Name	Eneida
	Suffix	
	Division	Departamento de Bioquímica, Instituto de Biologia
	Organization	Universidade Estadual de Campinas
	Address	Campinas, SP, Brazil
	Email	depaula@unicamp.br
Schedule	Received	
	Revised	
	Accepted	
Abstract	<p>Combined effects of flunitrazepam (FNZ) and lidocaine (LDC) were studied on the thermotropic equilibrium of dipalmitoyl phosphatidylcholine (dpPC) bilayers. This adds a thermodynamic dimension to previously reported geometric analysis in the erythrocyte model. LDC decreased the enthalpy and temperature for dpPC pre- and main-transitions (ΔH_p, ΔH_m, T_p, T_m) and decreased the cooperativity of the main-transition ($\Delta T_{1/2,m}$). FNZ decreased ΔH_m and, at least up to 59 μM, also decreased ΔH_p. In conjunction with LDC, FNZ induced a recovery of $\Delta T_{1/2,m}$ control values and increased ΔH_m even above the control level. The deconvolution of the main-transition peak at high LDC concentrations revealed three components possibly represented by: a self-segregated fraction of pure dpPC, a dpPC–LDC mixture and a phase with a lipid structure of intermediate stability associated with LDC self-aggregation within the lipid phase. Some LDC effects on thermodynamic parameters were reverted at proper LDC/FNZ molar ratios, suggesting that FNZ restricts the maximal availability of the LDC partitioned into the lipid phase. Thus, beyond its complexity, the lipid–LDC mixture can be rationalized as an equilibrium of coexisting phases which gains homogeneity in the presence of FNZ. This work stresses the relevance of nonspecific drug–membrane binding on LDC–FNZ pharmacological interactions and would have pharmaceutical applications in liposomal multidrug-delivery.</p>	
Keywords (separated by '-')	Flunitrazepam - Lidocaine - Dipalmitoyl phosphatidylcholine - Calorimetry - Liposomes - Thermotropic phase changes	
Footnote Information	Benjamin Caruso and Julieta M. Sánchez contributed equally to this work.	

Journal: 12013
Article: 9494



Author Query Form

**Please ensure you fill out your response to the queries raised below
and return this form along with your corrections**

Dear Author

During the process of typesetting your article, the following queries have arisen. Please check your typeset proof carefully against the queries listed below and mark the necessary changes either directly on the proof/online grid or in the 'Author's response' area provided below

Query	Details required	Author's response
	Please check and confirm the edit in the article title.	
	Please check and confirm that the authors and their respective affiliations have been correctly identified and amend if necessary.	
	As per the information provided by the publisher, Fig. 3 will be black and white in print; hence, please confirm whether we can add "colour figure online" to the caption.	

Probing the Combined Effect of Flunitrazepam and Lidocaine on the Stability and Organization of Bilayer Lipid Membranes. A Differential Scanning Calorimetry and Dynamic Light Scattering Study

Benjamín Caruso · Julieta M. Sánchez ·
Daniel A. García · Eneida de Paula ·
María A. Perillo

© Springer Science+Business Media New York 2012

Abstract Combined effects of flunitrazepam (FNZ) and lidocaine (LDC) were studied on the thermotropic equilibrium of dipalmitoyl phosphatidylcholine (dpPC) bilayers. This adds a thermodynamic dimension to previously reported geometric analysis in the erythrocyte model. LDC decreased the enthalpy and temperature for dpPC pre- and main-transitions (ΔH_p , ΔH_m , T_p , T_m) and decreased the cooperativity of the main-transition ($\Delta T_{1/2,m}$). FNZ decreased ΔH_m and, at least up to 59 μM , also decreased ΔH_p . In conjunction with LDC, FNZ induced a recovery of $\Delta T_{1/2,m}$ control values and increased ΔH_m even above the control level. The deconvolution of the main-transition peak at high LDC concentrations revealed three components possibly represented by: a self-segregated fraction of pure dpPC, a dpPC–LDC mixture and a phase with a lipid structure of intermediate stability associated with LDC

self-aggregation within the lipid phase. Some LDC effects on thermodynamic parameters were reverted at proper LDC/FNZ molar ratios, suggesting that FNZ restricts the maximal availability of the LDC partitioned into the lipid phase. Thus, beyond its complexity, the lipid–LDC mixture can be rationalized as an equilibrium of coexisting phases which gains homogeneity in the presence of FNZ. This work stresses the relevance of nonspecific drug–membrane binding on LDC–FNZ pharmacological interactions and would have pharmaceutical applications in liposomal multidrug-delivery.

Keywords Flunitrazepam · Lidocaine · Dipalmitoyl phosphatidylcholine · Calorimetry · Liposomes · Thermotropic phase changes

Abbreviations

BZD	Benzodiazepine
dpPC	Dipalmitoyl phosphatidylcholine
DSC	Differential scanning calorimetry
FNZ	Flunitrazepam
LDC	Lidocaine
MLVs	Multilamellar vesicles

Introduction

Benzodiazepines (BZDs) are widely used as anxiolytic, miorelaxant, hypnotic, and anticonvulsant drugs. Flunitrazepam (FNZ) is a potent anxiolytic BZD mainly used as a night-time hypnotic or in surgery, to induce anesthesia [1]. These drugs have a prominent role in general anesthesia not only because of their amnestic effects but also because of their anxiolytic actions [2]. In turn, local anesthetic agents

Benjamín Caruso and Julieta M. Sánchez contributed equally to this work.

B. Caruso · J. M. Sánchez · D. A. García · M. A. Perillo (✉)
Cátedra de Química Biológica, Departamento de Química,
FCEfYN, Instituto de Investigaciones Biológicas y Tecnológicas
(IIBYT), CONICET-Universidad Nacional de Córdoba, Av.
Vélez Sarsfield 1611, X5016GCA Córdoba, Argentina
e-mail: mperillo@efn.uncor.edu

B. Caruso
e-mail: bcaruso@efn.uncor.edu

J. M. Sánchez
e-mail: jmsanchez@efn.uncor.edu

D. A. García
e-mail: dagarcia@efn.uncor.edu

E. de Paula
Departamento de Bioquímica, Instituto de Biologia,
Universidade Estadual de Campinas, Campinas, SP, Brazil
e-mail: depaula@unicamp.br

(LA) can be defined as drugs which are used clinically to produce reversible loss of sensation in a circumscribed area of the body. They are usually of the amino amides class and include agents such as lidocaine (LDC), bupivacaine, prilocaine, mepivacaine, ropivacaine, and articaine [3, 4]. Many invasive procedures, such as plastic-surgery, are performed under local anesthesia, however, anxiety and apprehension can increase the severity of pain or discomfort experienced during the surgery. The use of local anesthesia with sedation offers to the patient more comfort and safety and, to the anesthesia personnel and the surgeon, great flexibility in tailoring the degree of anesthesia to the needs of the patient [5]. Hence, sedation and analgesia are often provided during local anesthesia [5–9] and, in addition, BZDs appear to protect against cerebral hypoxia and are very effective anticonvulsant agents against local anesthetic-caused seizures [9–12]. So, BZD and LA are often used simultaneously.

BZDs are known to affect the nervous transmission by interacting with specific membrane proteins [13, 14] such as the GABA_A receptor while LA acts mainly through voltage gated Na⁺ channels (r.f. [15]). However, due to their high lipophilicity, both drugs (BZDs and LA) are able to establish non-specific interactions with the lipid phase of the membrane [16, 17].

LDC, a well-known local anesthetic, diminishes the membrane organization of egg phosphatidylcholine (EPC) vesicles to a greater extent than other more hydrophobic local anesthetics such as etidocaine, bupivacaine, dibucaine, or tetracaine as revealed by electron paramagnetic resonance studies [18]. ¹H nuclear magnetic resonance studies showed that this effect was evident at the glycerol region, where the aromatic ring of the anesthetic was inserted, and also at the choline moiety of EPC (data from nuclear overhauser effect, NOE, cross-peak between the aromatic/LDC and choline hydrogens of EPC) [19]. By producing spaces in-between the lipid molecules LDC insertion in the polar head group region induces a less tight packing of the membrane, an effect that extends throughout the acyl chain of EPC in multilamellar vesicles (MLVs) and small unilamellar vesicles (SUVs), as shown by decreases in membrane organization through EPR, fluorescence, and ²H-NMR [20].

In turn, previous studies from our laboratory demonstrated that BZD-membrane non-specific interactions could be explained by a partition equilibrium model (unlimited incorporation of molecules) [16]. This is thermodynamically consistent with guest molecules accommodated between the lipid molecules, becoming part of the membrane [21] and may eventually lead to the swelling of the membrane until it is converted into a non-bilayer phase [21]. We have demonstrated that FNZ, as well as other BZDs, interacts with lipid membranes locating preferentially at the

phospholipid polar head group region, expanding the membrane [22–25]. This leads to an increase in the relative volume of the polar head group region and to a decrease in the stability of the self-aggregating structure, which is forced towards an increase in its surface curvature [25]. The tension in the bilayer structure generated through this mechanism could be relieved by diminishing the diameter of dipalmitoyl phosphatidylcholine (dpPC) MLVs, as demonstrated by molecular filtration [23] and transmission electron microscopy [25].

The relevance of these findings for the cellular biology was highlighted in a previous report [26], where using a well-accepted model to study drug-membrane interactions such as human red blood cell (hRBC) [27] we demonstrated that the individual effects of FNZ and LDC (echinocytosis and stomatocytosis, respectively) were a time- and concentration-dependent phenomenon and could be mutually compensated.

The morphology of a cell is highly determined by mechanochemical/viscoelastic properties which arise as the resultant of dynamic and possibly nonlinear interactions of many molecular fluxes (e.g., molecular movements from one monolayer to the other, insertion of solutes, asymmetry between the composition of the inner and outer aqueous media, etc.) [28]. Perturbation of those fluxes or of their conjugated forces (e.g., curvature tensions) will lead to changes in cellular morphology. Actually, any asymmetry in molecular species and/or other fields across the bilayer will result in a curved equilibrium configuration of the membrane [28–30]. This may work as a transducer mechanism of drug's effect exerted through membrane interaction. The combined effects of BDZs and LA have been studied in hRBC within this context [26]. However, the plasma membrane represents a supramolecular structure where not only the association of lipids and proteins in the bilayer, but also their interaction with the cytoskeleton, as well as with intercellular matrix components, take part in determining the surface curvature which is finally expressed on cell morphology. In such a complex scenario, it cannot be unequivocally stated which is the exact pathway followed by hRBC after the initial FNZ or LDC-membrane interaction, towards the shape change. Nevertheless, their concentration-dependent mutual compensating effects on hRBC shape, in addition to the proved ability of membrane-bound drugs (including FNZ and LDC) to induce lipid translocation [25, 27, 31] support the idea of a direct mechanical effect of both drugs on membrane curvature. The relief of those tensions would lead to organizational changes at the supramolecular level.

This work was aimed at better understanding the effect of FNZ and LDC on the stability and organization of membrane bilayers, by adding a thermodynamic dimension to the previous geometric analysis. The latter was based on the opposite effects of LDC and FNZ on the membrane

curvature (topology) in hRBC [26] and phospholipids translocation following drugs insertion according to their intrinsic molecular geometry (cone or cylindrical shape) and drugs localization within different regions of the bilayer [25, 26]. Hence, we studied the individual and combined effects of FNZ and LDC, within the same concentration range applied in the hRBC model, on the thermotropic equilibrium of dpPC bilayers by using high sensitivity differential scanning calorimetry (DSC). This work will contribute to the knowledge of drug's action mechanisms exerted through membrane interaction and may serve as a starting point in studies of pharmaceutical applications on liposomal multidrug-delivery.

Methods

Materials

FNZ (7-nitro-1,3-dihydro-1-methyl-5-(2-fluorophenyl)-1,4-benzodiazepin-2-one) was kindly supplied by Hoffman La Roche (Basle, Switzerland). LDC (2-diethylamino-*N*-(2,6-dimethylphenyl) acetamide) and dpPC were obtained from Sigma Chem. Co (St. Louis, MA). All other chemicals were of analytical grade. Chemical structures of FNZ and LDC are shown in Scheme 1.

Preparation of MLVs and drug incorporation

MLVs were prepared from a chloroform solution of dpPC. The solvent was evaporated under a stream of N₂ and the

sample was placed under vacuum for 1 h. The dry lipid film was suspended in 50 mM phosphate buffer pH 7.4 by six consecutive cycles of heating at ~50 °C for 2 min plus vortexing during 30 s. This heating temperature was above the gel-to-liquid-crystalline phase transition temperature of dpPC (i.e., 41.3 ± 1.8 °C [32]). In all cases, the dpPC final concentration was 1 mg/mL.

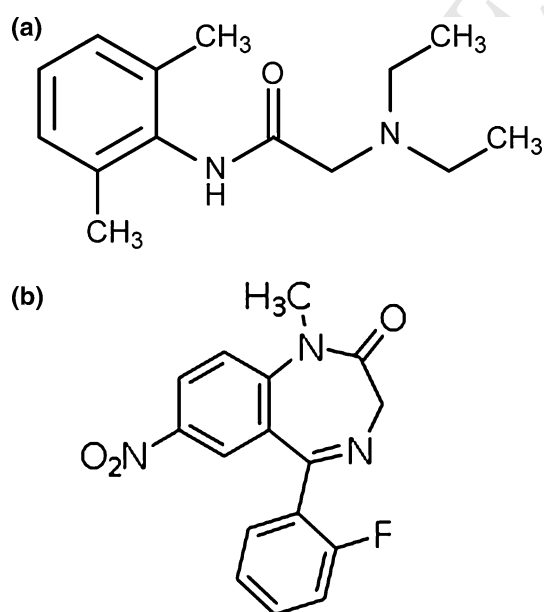
LDC and FNZ stock solutions were prepared in 50 mM phosphate buffer pH 7.4. Drugs were incorporated to the MLVs dispersion 10 min before the beginning of the thermal scanning, to a final drug concentration between 0.5 and 10 mM for LDC and 12 and 200 μM for FNZ.

DSC Experiments

DSC experiments were performed with a VP-DSC micro-calorimeter (MicrocalTM, Inc, Nothampton, MA). The degassed samples containing MLVs, in the absence or in the presence of drugs, were submitted to two heating/cooling cycles, from 20/25 to 60 °C, at a scanning speed of 1 °C/min. A rescan was done after each scan with a 15 min pre-scan incubation at 20/25 °C. The data were analyzed with DSC-specific software, ORIGIN[®] 5.0, provided by Microcal. The effects of FNZ and LDC, added together or separately to the dpPC vesicles, were evaluated through different parameters such as enthalpy change (ΔH_p , ΔH_m), transition temperature (T_p , T_m), and half-width of the transition peak ($\Delta T_{1/2p}$, $\Delta T_{1/2m}$). Subscripts *p* and *m* represent the pre- and main-transitions of dpPC, respectively. The thermotropic parameters ΔH and T are directly related to the sample stability, and $\Delta T_{1/2}$ is inversely related with the cooperativity of the phase-transition process. When required, calorimetric peak deconvolution was performed using PeakFit (Systat Software Inc., Chigago, IL).

Dynamic Light Scattering

Liposomes size distribution were determined by using a NicompTM 380 particle sizer (Nicomp Particle Sizer Systems, Santa Bárbara, CA) operating at 532 nm at an average count rate between 250 and 500 kHz; run time was around 15 min for most samples. DLS experiments were performed on MLVs of dpPC dispersed in buffer at a lipid concentration of 1 mg/ml, in the absence (MLV_{Buffer}) or in the presence of 10 mM LDC (MLV_{LDC}) alone or with the addition of 59 μM FNZ (MLV_{LDC/FNZ}). Measurements were made at 22 °C before and after submitting the samples to a temperature scan from 20 to 60 °C. The time autocorrelation function of scattered light intensities was analyzed by an inverse Laplace transform (ILS) algorithm to obtain a volume weighted distribution of diameters.



Scheme 1 Chemical structures of LDC (a) and FNZ (b)



237 **Results**238 **DSC Analysis of LDC and FNZ Stabilization Within**
239 **dpPC Bilayers**

240 Lipid bilayers, even those consistent of an assembly of
241 single pure phospholipids in excess water, can undergo
242 multiple phase transitions [32]. For dpPC, in a temperature
243 range between 0 and 50 °C, four lamellar phases can be
244 distinguished: L_c , $L_{\beta'}$, $P_{\beta'}$, and L_{α} . They are involved in the
245 sub-, pre-, and main phase transitions which are expressed as
246 $L_c \rightarrow L_{\beta'}$, $L_{\beta'} \rightarrow P_{\beta'}$, and $P_{\beta'} \rightarrow L_{\alpha}$, respectively. An
247 additional intermediate gel phase with interdigitated
248 hydrocarbon chains (L_{β}^{int}) intervening between the $L_{\beta'}$ and
249 $P_{\beta'}$ phases in dpPC has been reported to occur at high
250 hydrostatic pressures and also in the presence of ethanol,
251 some local anesthetics (dibucaine, tetracaine [33], LDC
252 [34]), and diterpenes [35]. Upon heating, L_{β}^{int} either trans-
253 forms directly into the L_{α} phase or follows a $L_{\beta}^{int} \rightarrow P_{\beta'}$
254 transition that precedes the $P_{\beta'} \rightarrow L_{\alpha}$, depending on the
255 mechanism that induced the L_{β}^{int} phase. Since the tempera-
256 ture range assayed usually starts at 25 °C, the sub-transition
257 is not registered in most works. Thus, a representative
258 thermogram of a first calorimetric scan of pure dpPC at an
259 external pressure of 1 atm shows two endothermic peaks
260 corresponding to pre- and main-transitions.

261 Figure 1 summarizes the main findings of the present work.
262 The thermogram of pure dpPC exhibits two endothermic
263 peaks which are displaced to lower temperatures and become
264 wider in the presence of 10 mM LDC alone. The addition of
265 59 μ M FNZ to the sample containing LDC, allows the main
266 peak to recover sharpness even though the former drug alone
267 seemed unable to induce a significant effect.

268 A deconvolution analysis on the main-transition peak of
269 dpPC in the presence of LDC without (Fig. 1b) or with
270 FNZ (Fig. 1c) resulted from the application of a non-two
271 state transition model. In the presence of LDC (Fig. 1b),
272 the main-transition peak appeared wider than in pure dpPC
273 and split into three components: two major ones at 39.55
274 and 40.43 °C. The third minor peak appeared at 41.46 °C,
275 and it would correspond to that of pure dpPC. Although
276 59 μ M FNZ induced only a marginal effect on the thermogram
277 of pure dpPC (see Fig. 1a), in samples containing
278 10 mM LDC it favored the non-two-state transition, with
279 three peaks (39.74, 40.52, and 41.20 °C) that, within the
280 experimental error, exhibited T_m values similar to those
281 observed in the presence of LDC alone, but with a pre-
282 vailing and higher cooperative contribution of the peak
283 with the lowest T_m (Fig. 1c).

284 A similar analysis was extended to samples containing
285 different LDC concentrations in the absence (Fig. 2a, d)
286 and in the presence (Fig. 2e–h) of FNZ. Three or four

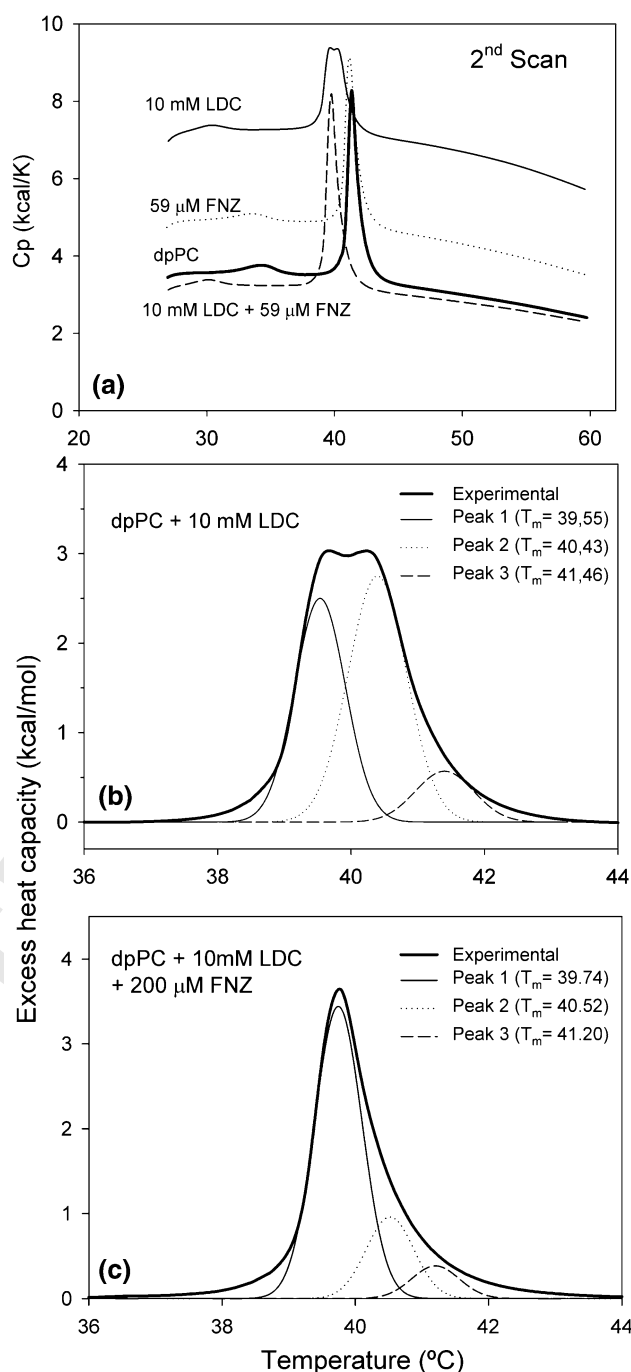
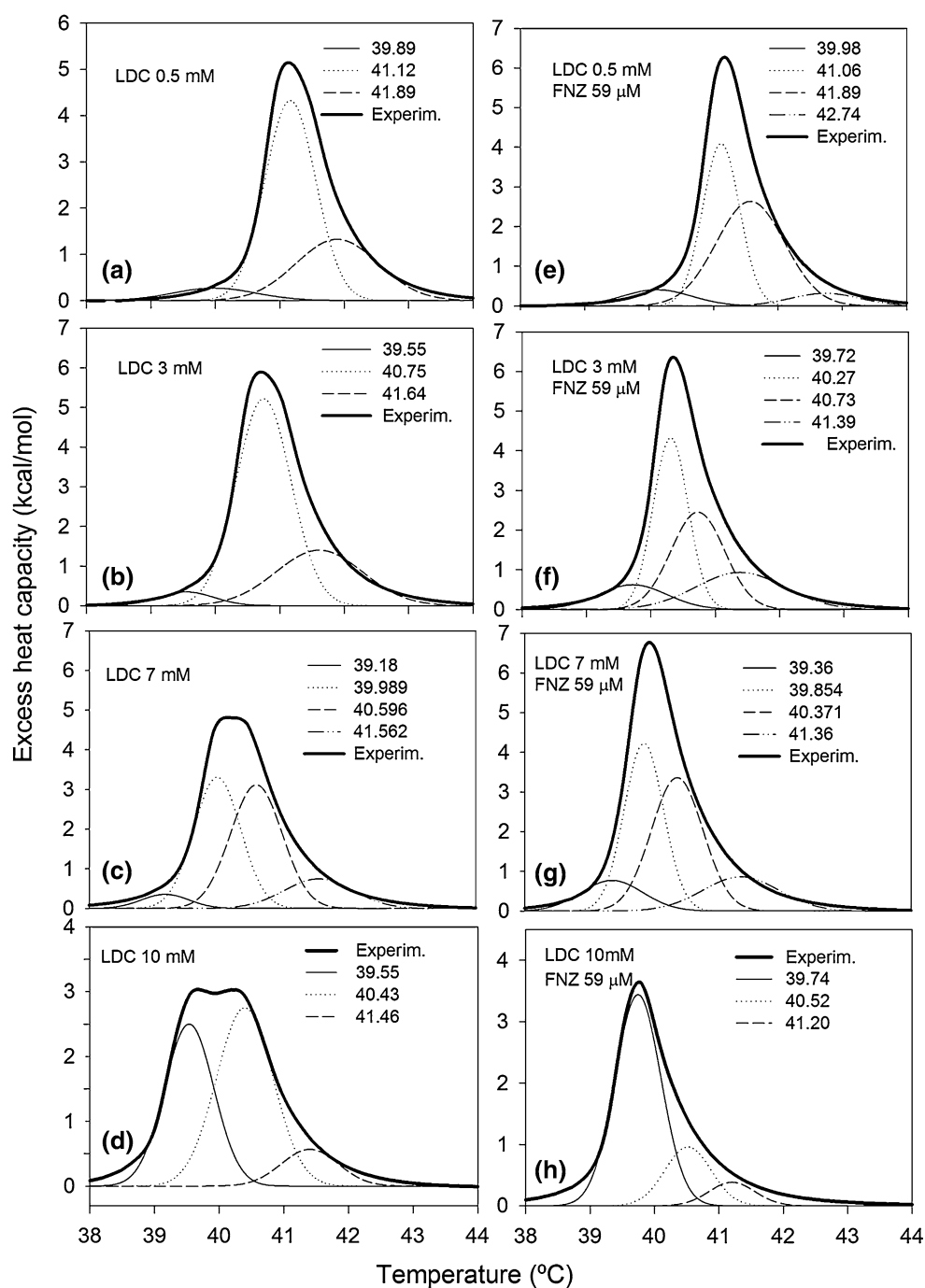


Fig. 1 **a** Individual and combined effects of FNZ and LDC on the thermotropic behavior of dpPC. In all cases, pH was maintained at 7.4 with 50 mM phosphate buffer. **b** Deconvolution of main-transition peak of dpPC in the presence of 10 mM LDC or **c** 10 mM LDC plus 200 μ M FNZ

peaks contributing in different proportions to the whole calorimetric transition could be resolved in the different samples. This information is summarized in Fig. 3, where in a temperature versus [LDC] plane, the occurrence of transition peaks (identified by their temperature values) appearing at each LDC concentration is plotted and

Fig. 2 Effect of LDC and FNZ on the component composition of the main-transition peak of dpPC thermogram. Drugs' concentrations and T_m values are indicated on the graphs. Deconvolution was performed using PeakFit (Systat Software Inc., Chicago, IL)



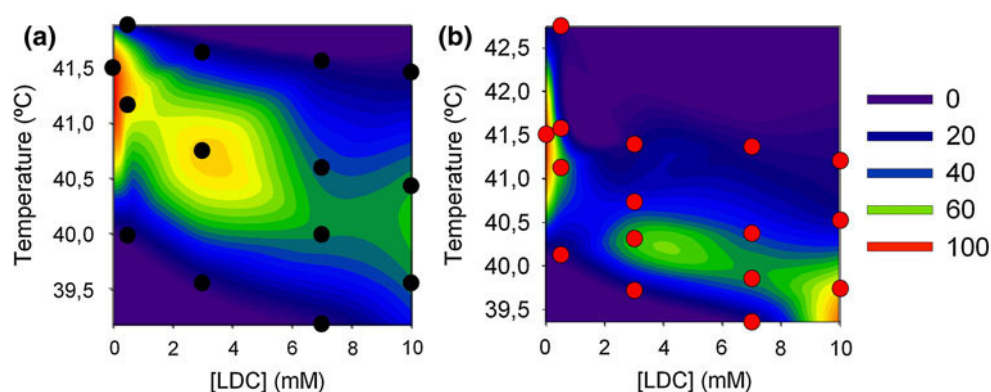
characterized by a color scale, according to their proportional contribution to the whole transition. Red corresponds to 100 % (single peak in the main-transition), while in split main-transitions lighter colors represent higher percentages. It can be observed that the largest peaks shift to lower temperatures as LDC concentration increases (Fig. 3a). This tendency becomes more marked in the presence of FNZ (Fig. 3b), and T_m values spread along a narrower range. At very low [LDC], in the presence of

FNZ, the main-transition exhibited a component at temperatures significantly above the T_m of pure dpPC.

These results suggested that LDC was unevenly dispersed within the bilayer making up a landscape of dpPC-LDC mixtures of different compositions and/or structures. These mixtures would coexist in different proportions with a segregated pure lipid phase, according to the intensity of a colligative effect or drug location within the membrane depth. However, this might also indicate that the mixture



Fig. 3 Temperature location and proportional contribution of peaks resulting from the deconvolution analysis of DSC thermograms of dpPC in the presence of varying LDC. **a** Without and **b** with 59 μ M FNZ. Color code reflects the percentage of each component contributing to the main-transition peak



could not be able to reach the equilibrium state due to kinetic restrictions. So, to investigate this possibility, sequential DSC scans in the heating and the cooling directions were also run.

Thermograms in the heating (scan and rescan) and cooling directions are shown in Fig. 4 and the calorimetric parameters determined are synthesized in Table 1. Under the present conditions, the pre-transition ($L_{\beta'} \rightarrow P_{\beta'}$ phase transition) of dpPC was observed as a fairly broad peak ($\Delta T_{1/2} = 2.3$ °C), centered near 35 °C on heating, and as a broader ($\Delta T_{1/2} = 2.7$ °C) peak of reduced area, centered at 30 °C on cooling. The main-transition ($P_{\beta'} \rightarrow L_{\alpha}$ phase transition) was centered at 41.65 °C on heating and at 40.6 °C on cooling and appeared as sharp peaks ($\Delta T_{1/2} \cong 1$ °C) in both scanning directions (Fig. 4a; Table 1). LDC increased the heating/cooling hysteresis (the pre-transition almost disappeared on cooling, Fig. 4b) and the addition of FNZ tended to revert this effect (Fig. 4c). Table 1 shows that the hysteresis in the heating/cooling cycle, for both transitions, increased with LDC (from 5.32 to 6.85 °C and from 1.05 to 1.35 °C for pre- and main-transition of pure dpPC, respectively) and then decreased with the addition of FNZ (to 6.55 and 0.88 °C, respectively). Successive scans were reproducible. Taken together, these results indicated that an equilibrium of coexisting mixtures can be reached in the presence of LDC, while in the presence of FNZ, the system becomes more homogeneous.

Effects of LDC and FNZ on the Thermodynamic Parameters

The second of two successive DSC scans of dpPC was analyzed in the presence of increasing concentrations of either LDC with or without 59 μ M FNZ (Fig. 5a–e) or FNZ with or without 10 mM LDC (Fig. 5f–i). FNZ and LDC concentrations chosen were a compromise between their aqueous solubility (1.4 M for LDC at pH 7.4 [36] and 0.25 mM for FNZ [37]), and their known effects on phospholipid vesicles revealed by calorimetric studies and

their mutual compensatory effects on the shape of hRBC [26]. In Fig. 5a–e, with the aid of lines drawn to guide the eye along T_p and T_m of pure dpPC, it is clearly observed a LDC concentration-dependent decrease in both transition temperatures as well as a decrease in the cooperativity of the main-transition (Fig. 5a–e). The addition of FNZ improved the cooperativity of the main-transition (peaks became thinner) (Fig. 5f). As shown in Fig. 5f, i, the effect of increasing FNZ concentrations in the absence of 10 mM LDC seems negligible. However, in the presence of 10 mM LDC, FNZ, at all the concentrations tested, clearly improved the cooperativity of the main-transition.

A more detailed analysis is depicted in Fig. 6 on the calculated thermotropic parameters which were submitted to ANOVA tests. The results obtained with pure dpPC agree well with those reported by other authors [32]. During the rescan, T_m and T_p values did not vary with respect to those obtained during the first heating (compare 1st and 2nd heating in Table 1). The individual and/or combined effects of LDC and FNZ can be analyzed as follows:

Effects of LDC

The most clear and consistent concentration-dependent effects of LDC observed were: (a) a decrease in ΔH_m and ΔH_p (Fig. 6a, d; black symbols), (b) a decrease in both pre- and main-transition temperatures (more noticeable on T_p) (Fig. 6b, e, black symbols), and (c) an increase in the $\Delta T_{1/2}$ of the main-transition (Fig. 6f), which were in agreement with the results of Ueda et al. [38]. Some of the effects of LDC, such as the decrease in ΔH_p and ΔH_m (Fig. 6a, d) and the increase in $\Delta T_{1/2,m}$ (Fig. 6f), could be reverted by 59 μ M FNZ (Fig. 6a–f, white symbols). When samples were cooled down and re-scanned, the thermotropic behavior of dpPC in the presence of LDC did not exhibit significant differences from that observed during the first scan except from an improvement in the reproducibility of the main-transition parameters (data not shown) and an

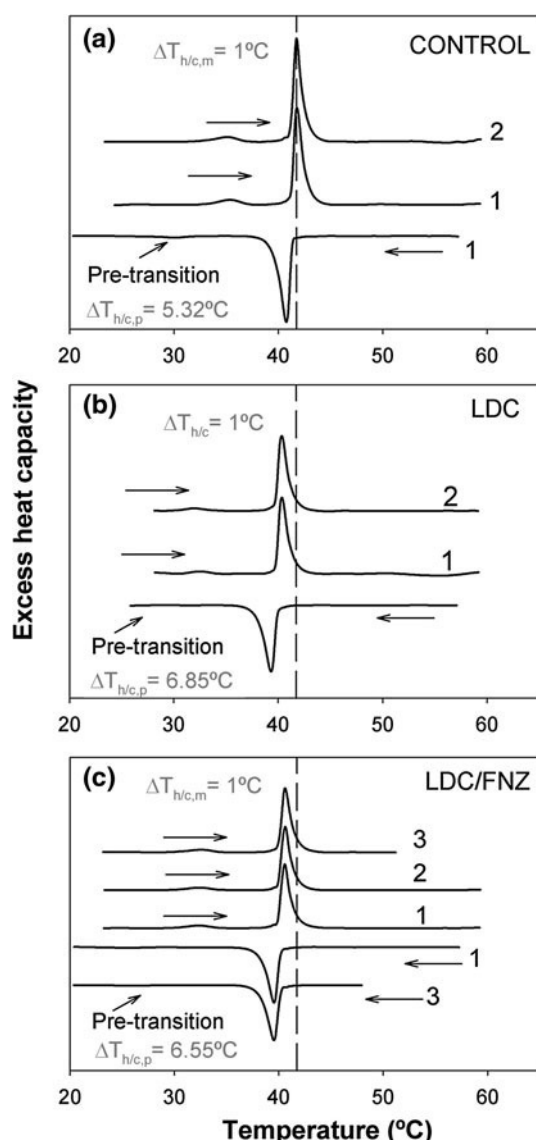


Fig. 4 Effect of LDC and LDC/FNZ on the DSC thermograms of dpPC recorded in the heating and cooling directions. Samples consisted of MLVs of dpPC dispersed in buffer (a), plus the addition of 10 mM LDC (b) or 10 mM LDC plus 59 μ M FNZ (c). Scanning rate was 1 $^{\circ}$ C/min. Horizontal arrows points towards the temperature scan direction and numbers refer to the sequential scan order. Vertical dashed lines mark the main-transition temperature of pure dpPC. $\Delta T_{h/c,m}$ and $\Delta T_{h/c,p}$, hysteresis within the heating and cooling cycle in the temperatures of the main- ($L_{\beta'}/P_{\beta'}$) and pre- ($P_{\beta'}/L_{\alpha}$) transitions, respectively

impairment of those of the pre-transition, which may be related with drugs homogenization within the structure of the bilayer upon membrane annealing.

Effects of FNZ

When the samples containing increasing concentrations of FNZ were scanned, a concentration-dependent decrease in the values of ΔH_p and ΔH_m was observed up to 59 μ M FNZ (Fig. 6g, j, black symbols). At concentrations above 59 μ M,

FNZ was able to revert the effect of 10 mM LDC on ΔH_m (Fig. 6j, white symbols) and $\Delta T_{1/2,m}$ (Fig. 6l, white symbols). Interestingly, in the sample containing 10 mM LDC plus 59 μ M FNZ, the ΔH_m was significantly higher than in the control (no drug added) (Fig. 6j). On the other hand, the effects of LDC on the values of ΔH_p (Fig. 6g) and the position of pre- and main-transition peaks (T_p , T_m , Fig. 6h, k) as well as the width of the pre-transition peak ($\Delta T_{1/2,p}$, Fig. 6i) could not be reverted by FNZ within the concentration range studied. Upon the addition of FNZ to samples containing LDC, the heating/cooling hysteresis in the $L_{\beta'} \rightarrow P_{\beta'}$ phase transition followed and opposite trend compared to what was observed in the presence of LDC alone, partially reverting the effects of the anesthetic (Fig. 4c; Table 1).

From the lipid–water partition coefficient values between EPC MLVs and water at pH 7.4 ($P_{LDC} = 76$ at 25 $^{\circ}$ C [39] and $P_{FNZ} = 30$ at 32 $^{\circ}$ C [40]), it can be roughly calculated that the ratio between LDC and FNZ molar concentrations in the membrane ($[LDC]_m/[FNZ]_m$) varied within the range 21–439 or 1,055–126 in the experiments done at 0.5–10 mM [LDC] at a constant [FNZ] (Figs. 5a–e, 6a–f) and in those where [FNZ] varied between 12 and 200 μ M at constant [LDC] (Figs. 5f–i; 6g–l), respectively. Considering that the values for thermodynamic parameters were plotted as a function of $[LDC]_m/[FNZ]_m$ ratio (Fig. 6m–r) to reveal that up to a value of approximately 300, 59 μ M FNZ was able to revert LDC effects.

Effect of LDC and FNZ on the Size Distribution of dpPC MLVs

Samples analyzed were pure dpPC (MLV_{Buffer}), dpPC-containing 10 mM LDC (MLV_{LDC}) and dpPC containing 10 mM LDC with 59 μ M FNZ (MLV_{LDC-FNZ}). In general, vesicles distributed within three ranges of diameter lengths (d): $d < 100$ nm (Peak 1), 100 nm $< d < 1$ μ m (Peak 2) and 1 μ m $< d < 7.5$ μ m (Peak 3) (Fig. 7a) which were present in different proportions (Fig. 7b). Initially the three populations were present in MLV_{Buffer} as well as in MLV_{LDC/FNZ} although the smallest ones represented a very low proportion (< 3 %). In MLV_{LDC}, particles with the intermediate size were not detected. After heating, the middle size population appeared in MLV_{LDC} reaching 4 % and increased significantly in MLV_{LDC/FNZ}—up to 40 % (Fig. 7b). Note that changes occurred towards the direction of decreasing size and homogenization in size distribution of the vesicles.

Discussion

This work is a contribution to the drug–membrane interaction problem which is involved in the understanding of

Table 1 Analysis of DSC data of dpPC in the absence or in the presence of 10 mM LDC, with or without 59 μ M FNZ

Sample	Scanning direction	Pre-transition			Main-transition		
		ΔH (kcal/mol)	T_p ($^{\circ}$ C)	$\Delta T_{h/c,p}$ ($^{\circ}$ C)	ΔH (kcal/mol)	T_m ($^{\circ}$ C)	$\Delta T_{h/c,m}$ ($^{\circ}$ C)
dpPC	1st heating	0.73	35.32	5.32	6.95	41.65	1.05
	Cooling	0.29	30.00		6.87	40.60	
	2nd heating	0.77	35.04		7.13	41.70	
dpPC	1st heating	0.29	32.50	~ 6.85	5.7	40.50	1.35
10 mM LDC	Cooling ^a	nd	~ 25.65		5.7	39.16	
	2nd heating	0.35	31.82		5.7	40.48	
dpPC	1st heating	0.71	32.25	6.55	8.2	40.58	0.88
10 mM LDC	Cooling	0.25	25.70		7.87	39.70	
59 μ M FNZ	2nd heating	0.77	32.31		7.85	40.60	
	3rd heating	0.70	32.50	6.50	8.1	40.50	0.86
	3rd cooling	0.22	26.00		8.0	39.64	

MLVs of dpPC were dispersed in 50 mM phosphate buffer pH 7.4 containing or not 10 mM LDC or 10 mM LDC plus 59 μ M FNZ. Parameters were determined on data shown in Fig. 4. DSC scans within the 20–60 $^{\circ}$ C temperature range were performed at a 1 $^{\circ}$ C/min scanning rate. ΔT values for the control were similar to those reported previously at 0.17 $^{\circ}$ C/min scanning rate [54]. $\Delta T_{h/c,p}$ and $\Delta T_{h/c,m}$ reflect the hysteresis in the pre- (p) and main- (m) transitions, respectively, within the heating and cooling cycle

^a The intensity of the pre-transition peak in this case was very low so that the value of T_p determined is approximate

the activity of many therapeutic agents as well as their eventual liposome-mediated delivery. One of the challenges faced here is the analysis of the joint interaction of two drugs which combined administration finds relevant therapeutic applications. The thermodynamic approach provided information about the drugs relative concentrations allowing their permanency within the bilayer.

For the analysis of the results obtained, it is important to recall that at the pre-transition temperature, the polar heads of the phospholipid molecules get disordered [41], while the hydrocarbon chains appear to be ordered and assembled in a bi-dimensional network. This behavior is due to the fact that all hydrocarbon chains maintain an all-*trans* conformation and the resultant distance between them favors van der Waals attraction forces. When the temperature increases, the acyl chains arrangement is lost because of *trans* \rightarrow *gauche* isomerization between the hydrocarbon chains, which takes place at the main phase transition. The pre-transition is mainly affected by electrostatic interactions at the polar head group while the main-transition can be affected by pressure, pH, and membrane composition.

Effects on ΔH

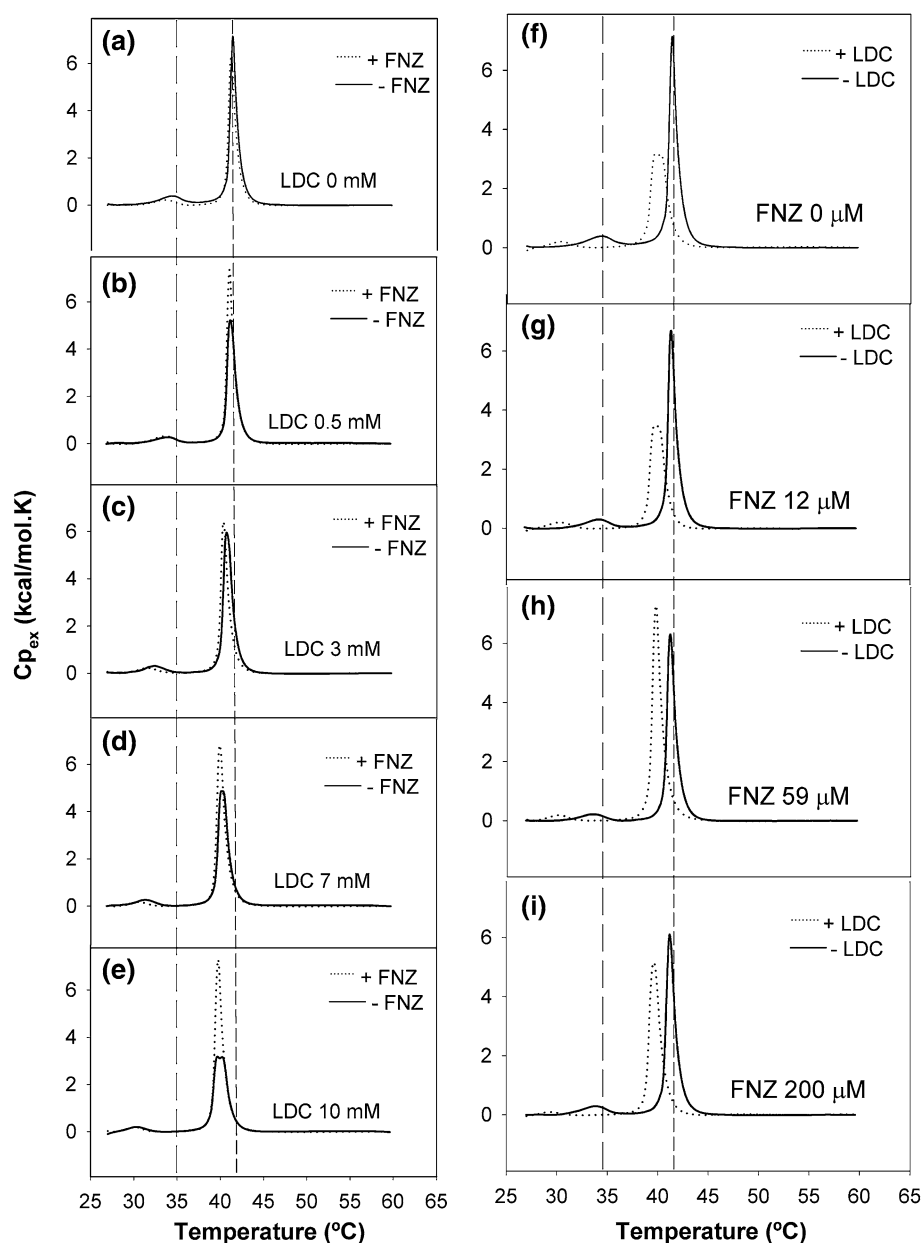
In a bilayer system where the stabilizing role of its water network at the lipid–water interface has been weakened, it would be expected a decrease in the amount of energy required for its phase transition. Accordingly, in the present work, the values of ΔH_p and ΔH_m for the pre- and main-transitions of dpPC, respectively, decreased in the presence of LDC (Fig. 6a, d) and, at a lesser extent, in the presence

of FNZ (Fig. 6g, j). Taking into account the above considerations and, in order to explain the effects on ΔH , four situations can be hypothesized:

Change in Vesicle Size

The size of the lipid self-aggregating structure also affects ΔH , decreasing the values of ΔH_p and ΔH_m of dpPC up to 900 and 30 %, respectively, when going from MLVs to SUVs [42]. During LDC partitioning, due to an active incorporation process, there is an initially high asymmetry in drug molecules distribution along the membrane width which, in addition to its well-documented location at the polar head group region [19], is expected to affect the surface curvature [21]. This would generate a tension that would be relieved through a generalized molecular reorganization into vesicles of smaller size. Supporting this hypothesis, it was demonstrated previously that, in the presence of 73.8 mM LDC, large unilamellar vesicles (LUVs) suffered a decreased in their diameter from 292 ± 4 to 227.0 ± 2.35 nm [43]. FNZ at a concentration of 100 μ M was also reported to be capable of reducing the size of dpPC MLVs [25] according to its localization at the polar head group membrane region [22, 24]. Not only the partition coefficients but also the depth of drug location inside the bilayer is known to increase with the temperature rise [24, 44, 45]. This may enhance effects on membrane curvature and particle size. So, in this work, we observed that the temperature-scan induced an increase in the abundance of the vesicles population of intermediate size in MLV_{LDC} as well as in $MLV_{LDC/FNZ}$ (Fig. 7) which

Fig. 5 DSC thermograms of dpPC in the presence of LDC, FNZ, or both. dpPC in the presence of LDC (a–e: 0, 0.5, 3, 7, 10 mM), containing (dotted lines) or not (dashed lines) 59 μ M FNZ and dpPC in the presence of increasing concentrations of FNZ (i–f: 0, 12, 59, and 200 μ M), containing (dotted lines) or not (dashed lines) 10 mM LDC. Lines passing through T_p and T_m of pure dpPC were drawn to guide the eye. Baselines were subtracted. All data shown correspond to second scans recordings



is correlated with an effect in the ΔH -concentration plot (Fig. 6m). Hence, macroscopically the effects of drugs were evidenced through the appearance of vesicles smaller in size and exhibiting a more homogeneous size distribution. This would be relevant for LDC–FNZ co-encapsulation in liposomes for pharmaceutical applications.

Impairment of Choline–Phosphate Electrostatic Interactions of Adjacent Lipids

This action should also be considered as a mechanism to explain the ΔH_p decrease as a function of LDC (Fig. 6a,

black symbols) [19, 45] as well as FNZ (Fig. 6g) concentrations.

Anesthetic–Anesthetic Intermolecular Interaction

Two theoretical models of lipid–anesthetic interactions predicting a concentration dependent increase in ΔH can be found in the literature [46, 47]. One of them is an interstitial model that considers only perturbations in the head-group region of the bilayer plus direct interactions between neighboring anesthetic molecules. The other model takes into account both van der Waals' and Coulombic interactions. LDC do not self-aggregate in aqueous media;



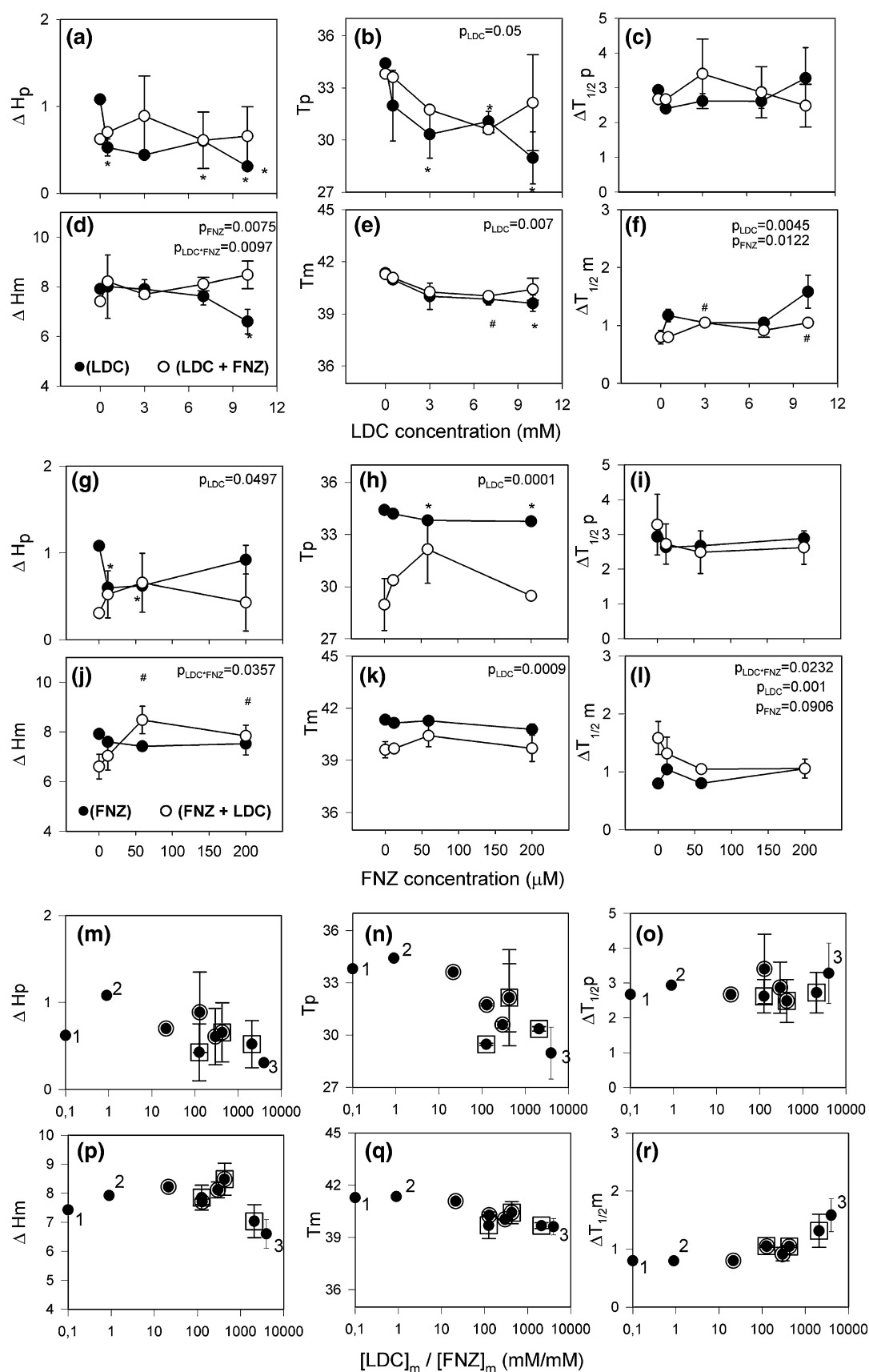


Fig. 6 Combined effects of LDC and FNZ on the calorimetric parameters ΔH , T , and $\Delta T_{1/2}$. **a–f** Effect of increasing concentrations of LDC alone (filled circle) or in conjunction with 59 μM FNZ (open circle). **g–i** Effect of increasing concentrations of FNZ alone (filled circle) or in conjunction with 10 mM LDC (open circle). Drugs were added 10 min before starting the first scan. The letters *p* and *m* after ΔH , T , and $\Delta T_{1/2}$ indicate pre- and main-transitions, respectively. In **a–f** (asterisk) indicates a significant difference from 0 mM LDC (filled circle) and (hash) indicates a significant difference from 0 mM LDC plus 59 μM FNZ (open circle); in **g–i** (asterisk) indicates a significant difference from 0 μM FNZ (filled circle) and (hash) indicates a significant difference from 0 μM FNZ plus 10 mM LDC (open circle) after one-way ANOVA and Duncan tests. *P* values result from two-way ANOVA considering both [FNZ] and [LDC] as sources of variation. $P < 0.05$ was considered statistically significant. **m–r** Thermodynamic parameters versus LDC/FNZ molar ratio in the membrane (m). Points 1, 2, and 3 refer to Control (no drug added), 59 μM FNZ and 10 mM LDC, respectively. Points enclosed in a circle or in a square correspond to samples containing 59 μM FNZ or 10 mM LDC, respectively, plus the other drug at the LDC/FNZ ratio indicated in the x axis

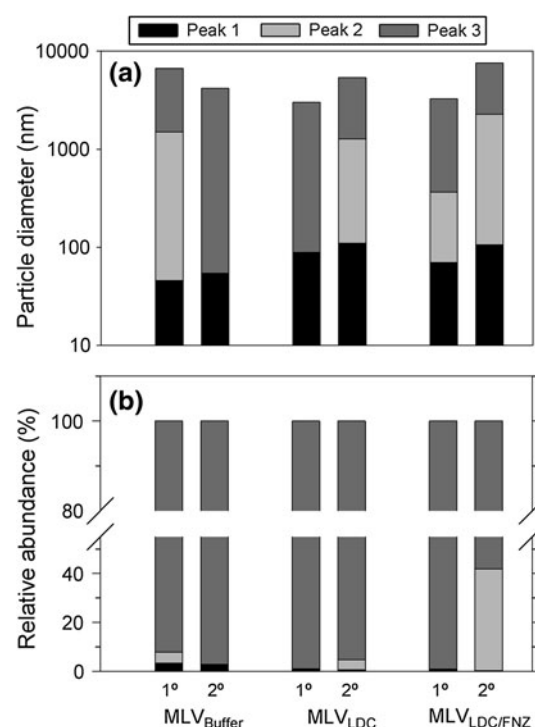


Fig. 7 Size distribution analysis by dynamic light scattering in MLVs of dpPC in the absence (MLV_{Buffer}) and in the presence of 10 mM LDC (MLV_{LDC}) or 10 mM LDC + 59 μM FNZ (MLV_{LDC/FNZ}). **a** Three peaks were identified in each sample with diameters $d < 100$ nm (Peak 1), $100 \text{ nm} < d < 1 \mu\text{m}$ (Peak 2) and $d < 7.5 \mu\text{m}$ (Peak 3). **b** Frequency distribution of peaks 1, 2, and 3 among different samples. Measurements were made at 22 °C before (1°) and after (2°) submitting the samples to a temperature scan from 20 to 60 °C

however, LDC–LDC interaction in the lipid media cannot be excluded (such a behavior was described for the local anesthetics carane, dibucaine and tetracaine) [48–50]. At high concentrations of the anesthetic, LDC–LDC aggregation may be accompanied by partial lipid segregation. This is supported by the peak at the highest T_m resulting from the deconvolution of the thermogram shown in Fig. 1b (see also Fig. 2a–d) which may be assigned to a pure lipid phase. In this condition, LDC–LDC interactions may be favored generating packing defects and tensions that can be relieved through structural rearrangement such as the induction of an interdigitated phase (see below). This phenomenon may have been potentiated by FNZ (Fig. 6j, 3b). Thus, FNZ would restrict the maximal availability of the LDC partitioned within the bilayer. This can be conceived as part of LDC molecules being expelled from the bilayers (reduced amount of drug) or confined in self-aggregated structures (reduced liposome–water transference rate leading to lower water solubility, hence less availability).

An Interdigitated-Lamellar Phase Change

The most characteristic calorimetric feature associated with this phase is a pronounced increase in the molar enthalpy of the main lipid phase transition. A concentration-dependent increase in ΔH might be related with the interstitial location of solutes within the lipid lattice, causing cavities between chains in the bilayer interior. Since the energy of formation of those cavities is extremely large, they have to be eliminated through an interdigitation of the chains. The ΔH for interdigitated-lamellar phase change increases with solute concentration. This tendency has been demonstrated for several local anesthetics including LDC, through DSC experiments [33] as well as by SAXS [34]. In the present

experimental condition, such high local concentration may be reached in the outer lamellas of MLVs at a relative low total LDC concentration. Hence, a FNZ-induced growth of ΔH_m above the control values occurred at proper LDC/FNZ molar ratios (Fig. 6d, j). Molecular rearrangements and/or drug redistribution in the bilayers were suggested by the FNZ mediated change in the peak composition derived from the deconvolution analysis (Fig. 1c) being also a LDC concentration dependent phenomenon (Figs. 2, 3). Furthermore, it is interesting to note that the increase in the heating/cooling hysteresis in the $L_{\beta'} \rightarrow P_{\beta'}$ phase transition induced by LDC and LDC/FNZ also supports this mechanism of drug–membrane interaction (Fig. 4; Table 1) as hysteresis of phase transitions is considered a “strong” evidence of the existence of interdigitated phases [35].

From these situations, it could be argued that vesicle size reduction (hypothesis a) and the concomitant effects on increasing surface curvature and impairing lipid–lipid interaction at the polar head group (hypothesis b) may be proposed as the mechanisms to explain the decreasing tendency induced by LDC on ΔH_p and ΔH_m in the plots



shown in Fig. 6a, d, black symbols. The reversing effects of FNZ (Fig. 6a, d, g, j, white symbols) would be associated with the induction of LDC segregation at the lipid phase (hypothesis c). The rate of membrane deformations involving bilayer expansion and extension may be damped by the hydrodynamics of the adjacent water compartments. However, membrane bending and relaxation may be rate limited by viscous drag between the monolayers. This will depend on how tightly the two layers of the bilayer are coupled (e.g., degree of interdigitation between acyl chains—hypothesis d) [51]. All the mechanisms (hypothesis a–d) may work in conjunction for the recovering of ΔH values of pure lipid phase transitions.

Effects on Phase Transition Temperatures and Cooperativity

Inoko and Mitsui [52] provided the information that the increase in the repeat distance of lamellar phase in a dpPC–water system at the pre-transition is due to the increase in the thickness of the water layer, indicating that the incorporation of additional water between the bilayers takes place at the pre-transition. Hence, the $P_{\beta'}$ phase has been accepted as the intermediate phase between the pre- and the main-transition, and it was associated with the cooperative interaction between the polar head groups of dpPC and ‘newly incorporated water’ at the pre-transition [53]. So, drugs locating at the polar head group region are expected to disturb the hydration network at the interface and consequently to affect mainly the pre-transition phase change in dpPC. In addition, the thermodynamic equation expressing the colligative depression in the phase-transition temperature includes the transition enthalpy in the denominator. Since the enthalpy change for the pre-transition is significantly smaller than that for the main-transition, the depression of the T_p is expected to be amplified (Fig. 6b, h). From this point of view, the results obtained in this work with increasing concentrations of LDC and FNZ are consistent with this rationale as well as with the results reported by other authors [38, 46, 47]. The fact that the effects of FNZ on these parameters are more moderate than those exerted by LDC results from the narrower drug concentration-range used and lower partition coefficient of the former, and also from the different kind of interactions each drug establish with the dpPC–water interface (i.e., at pH 7.4, the largest part of LDC molecules are in a charged form— $pK_{LDC} = 7.8$ [54], while FNZ is neutral— $pK_{FNZ} = 1.8$ [22]).

In agreement with the results obtained by Ueda et al. [38], a previous heating allowed LDC to become more uniformly and deeply distributed in the interior of the multilamellar structure, increasing its effect on T_p depression (Fig. 6b, black symbols). LDC was effective in

diminishing the cooperativity of the phase transitions process, evidencing its inhibitory effect on the formation of hydrogen bonds (Fig. 6c, black symbols). Again, the effect of FNZ alone on this parameter was negligible (compare Fig. 6c, i, black symbols), due to the same reasons given for the effect on T_p .

If we accept that FNZ induced a segregation of LDC in the lipid phase (see hypothesis c) and the possibility that LDC aggregates formed inside of the bilayer structure could induced big structural tensions capable of being relieved through interdigitation (hypothesis d), then the reversal of LDC effects observed in the presence of 59 μ M FNZ (Fig. 6a, c, d, white symbols) as well as the recovery of ΔH_m control levels in the presence of 10 mM LDC plus 59 μ M FNZ or higher concentrations (Fig. 6j, white symbols), could be explained.

Significance of Drug Effects on Membrane Organization and Function

The correlation between the present combined effects of LDC and FNZ, and those found previously in the hRBC model are not straightforward because MLVs lack: (i) the asymmetry in composition between both lamellae in each bilayer, making ineffective the lipid flip–flop as a mechanism to compensate the tensions generated by drug incorporation, and (ii) the electrically negative internal membrane surface which enables the positively charged LDC molecule to be translocated and trapped in the internal monolayer, inducing a negative curvature of the whole membrane. However, the present experiment setup permits to separate the mechanical contribution of the combined mechanical/electrostatic effects expressed in hRBC.

For a symmetrical bilayer like MLVs, e.g., a bilayer composed of monolayers with identical values for the spontaneous curvature, the net spontaneous curvature will be zero because the tendencies to bend the layers are equal and opposite, and therefore will cancel between one another. However, the component layers will be under non-uniform tension arising from the frustrated spontaneous curvature. This kind of tensions is likely to express itself in a modified partitioning of amphiphiles and possibly also in the activity of membrane-embedded integrated proteins. The energy of inserting amphiphilic molecules into bilayers is a potential manifestation of lateral pressure in the membrane [45]. In this sense, previous studies on the hRBC model suggested a partitioning of LDC in the inner leaflet of the hRBC to satisfy the electrostatic differences: LDC positively charged on a negative interface [55]. However, the different curvatures of the inner and outer membrane leaflets may have played a role on this partitioning.

The main accepted action mechanism for LDC and FNZ involves their binding to specific proteins, the

voltage-gated Na^+ channel and the GABA_A receptor, respectively. Though, their ability to affect general membrane properties cannot be neglected. This fact suggests mechanisms that can explain possible secondary effects like those described above as well as eventual pharmacological interactions between them.

Conclusions

Through high sensitivity DSC, we studied the individual and combined effects of FNZ and LDC on the thermotropic equilibrium of dpPC bilayers, within a similar range used previously in the hRBC model. The results suggested that LDC was unevenly dispersed within the bilayer leading to dpPC–LDC mixtures of different compositions and/or structures. This was revealed by the non-two state mechanism associated to the main-transition as reflected by the several components of the transition peak identified through a deconvolution analysis. The proportion of each component was in accordance with the intensity of a coligative effect (associated with drug concentration) or drug location within the membrane depth (mainly dependent on temperature). From the values of thermodynamic parameters, it can be proposed that the coexisting phases are: a self-segregated fraction of pure dpPC, a dpPC–LDC mixture and a lipid phase of intermediate stability, possibly triggered by LDC self-association within the lipid phase. The latter was reverted in the presence of proper LDC/FNZ molar ratios, suggesting that FNZ favored the insertion of LDC within the lipid phase. T_m values and the heating/cooling hysteresis in the pre-transition reflected modifications in the lipid microstructure compatible with a FNZ facilitation of interdigitated phase induction.

Beyond its complexity, the lipid–LDC mixture can be rationalized as an equilibrium of coexisting phases which gains homogeneity in the presence of FNZ. Macroscopically, the effects of drugs were evidenced through the appearance of vesicles smaller in size and exhibiting a more homogeneous size distribution. In conjunction, this supports the possibility of LDC–FNZ co-encapsulation in liposomes for pharmaceutical uses. Typical sedative doses of FNZ (1 mg/70 kg body weight) leads to 6.5–8 ng/ml plasma concentrations [56–58], while typical LDC plasma concentrations for local nerve blockade range from 0.75 [59] to 1.35–5 $\mu\text{g/ml}$ [59–61]. Simultaneous administration of both drugs has also been reported [61], and taking into account the information provided by these authors (plasma concentration of LDC and dose of FNZ) [61] plus data from other literature sources [57], allow calculate that LDC/FNZ molar ratio in plasma was within 657 and 877, which corrected for the partition coefficients ($P_{\text{LDC}} = 76$ and $P_{\text{FNZ}} = 30$) correspond to 904–2,221 molar ratio in

membrane. The later values were calculated in our experiments starting from concentrations 1,000 times higher in the dispersant medium. This would suggests that a similar liposome preparation co-encapsulating LDC and FNZ would be able to provide therapeutically relevant plasma levels of both drugs after a 1/1,000 dilution which is achievable in practice. Further studies on liposome loading will be required to evaluate the relative and maximal concentrations allowed. In spite of this, up to our knowledge, this is the first time the effect of two drugs over model membranes can be distinguished to such point.

Concluding, this work contributes to stress the relevance of drug–membrane binding on LDC–FNZ pharmacological interactions and may help understanding and improving procedures of pharmaceutical importance in the field of drugs co-encapsulation in liposomes.

Acknowledgments This work was partially financed with grants from a bilateral CAPES (Brasil)/SPU(Argentina) project (# Project CAPG-BA 06/02), Fapesp (# 06/00121-9), SeCyT-UNC, Mincyt-Córdoba and CONICET (Argentina). JMS, DAG, and MAP are career investigators from CONICET and BC holds a postdoctoral fellowship from the later institution. EP has a fellowship from CNPq/Brazil. Authors gratefully acknowledge Dr M. L. Bianconi from UFRJ (Brazil) for the help with DSC experiments at the early stages of this work.

References

- Sloan, J. W., Martin, W. R., & Wala, E. P. (1991). A comparison of the physical dependence inducing properties of flunitrazepam and diazepam. *Pharmacology, Biochemistry and Behavior*, 39(2), 395–405.
- Smith, C. (1994). Pharmacology of local anaesthetic agents. *British Journal of Hospital Medicine*, 52(9), 455–460.
- Rudolph, U., & Möhler, H. (2004). Analysis of GABAA receptor function and dissection of the pharmacology of benzodiazepines and general anesthetics through mouse genetics. *Annual Review of Pharmacology and Toxicology*, 44, 475–498.
- McLure, H. A., & Rubin, A. P. (2005). Review of local anaesthetic agents. *Minerva Anestesiologica*, 71, 59–74.
- Biswas, S., et al. (1999). Low-dose midazolam infusion for oculoplastic surgery under local anesthesia. *Eye (Lond)*, 13(Pt 4), 537–540.
- Deng, X., et al. (2001). The use of midazolam and small-dose ketamine for sedation and analgesia during local anesthesia. *Anesthesia and Analgesia*, 93(5), 1174–1177.
- Cinnella, G., et al. (2007). Sedation analgesia during office-based plastic surgery procedures: Comparison of two opioid regimens. *Plastic and Reconstructive Surgery*, 119(7), 2263–2270.
- Badrinath, S., et al. (2000). The use of a ketamine-propofol combination during monitored anesthesia care. *Anesthesia and Analgesia*, 90(4), 858–862.
- Neal, J. M., et al. (2010). ASRA practice advisory on local anesthetic systemic toxicity. *Regional Anesthesia and Pain Medicine*, 35(2), 152–161.
- Rudolph, H., et al. (1981). Benzodiazepines protect mice from local anesthetic convulsions and deaths. *Anesthesia and Analgesia*, 60(6), 385–389.
- Hogan, Q. (1996). Local anesthetic toxicity: An update. *Regional Anesthesia*, 21(6), 43–50.

12. Weinberg, G. L. (2010). Treatment of Local Anesthetic Systemic Toxicity (LAST). *Regional Anesthesia and Pain Medicine*, 35(2), 188–193.
13. Gavish, M., et al. (1992). Biochemical, physiological, and pathological aspects of the peripheral benzodiazepine receptor. *Journal of Neurochemistry*, 58(5), 1589–1601.
14. Stephenson, F. A. (1998). Understanding the GABAA receptor: A chemically gated ion channel. *Biochemical Journal*, 249, 21–32.
15. Weinkauff, B., et al. (2012). Differential effects of lidocaine on nerve growth factor (NGF)-evoked heat- and mechanical hyperalgesia in humans. *European Journal of Pain*, 16(4), 543–549.
16. Perillo, M. A., & Arce, A. (1991). Determination of the membrane-buffer partition coefficient of flunitrazepam, a lipophilic drug. *Journal of Neuroscience Methods*, 36(2–3), 203–208.
17. Perillo, M., Garcia, D. A., & Arce, A. (1995). Partitioning of 1,4 benzodiazepines into natural membranes. *Molecular Membrane Biology*, 11, 217–224.
18. de Paula, E., & Schreier, S. (1995). Use of a novel method for determination of partition coefficients to compare the effect of local anesthetics on membrane structure. *Biochimica et Biophysica Acta*, 1240, 25–33.
19. Fernandes Fraceto, L., et al. (2002). Spectroscopic evidence for a preferential location of lidocaine inside phospholipid bilayers. *Biophysical Chemistry*, 99(3), 229–243.
20. de Paula, E., et al. (2008). Preferential location of lidocaine and etidocaine in lecithin bilayers as determined by EPR, fluorescence and ²H NMR. *Biophysical Chemistry*, 132(1), 47–54.
21. Seelig, A., Allegrini, P. R., & Seelig, J. (1988). Partitioning of local anesthetics into membranes: Surface charge effects monitored by the phospholipid head-group. *Biochimica et Biophysica Acta*, 939(2), 267–276.
22. García, D. A., & Perillo, M. A. (1997). Localization of flunitrazepam in artificial membranes. A spectrophotometric study about the effect the polarity of the medium exerts on flunitrazepam acid-base equilibrium. *Biochimica et Biophysica Acta*, 1324(1), 76–84.
23. García, D. A., & Perillo, M. A. (1997). Partitioning of flunitrazepam into model membranes studied by temperature controlled gel filtration chromatography. *Biomedical Chromatography*, 11(6), 343–347.
24. García, D. A., & Perillo, M. A. (1999). Benzodiazepine localization at the lipid–water interface: Effect of membrane composition and drug chemical structure. *Biochimica et Biophysica Acta*, 1418(1), 221–231.
25. Perillo, M. A., & Garcia, D. A. (2001). Flunitrazepam induces geometrical changes at the lipid–water interface. *Colloids and Surfaces B: Biointerfaces*, 20(1), 63–72.
26. García, D. A., Quiroga, S., & Perillo, M. A. (2000). Flunitrazepam partitioning into natural membranes increases surface curvature and alters cellular morphology. *Chemico-Biological Interactions*, 129(3), 263–277.
27. Chen, J. Y., & Huestis, W. H. (1997). Role of membrane lipid distribution in chlorpromazine-induced shape change of human erythrocytes. *Biochimica et Biophysica Acta*, 1323(2), 299–309.
28. Cullis, P. R., et al. (1997). Influence of pH gradients on the transbilayer transport of drugs, lipids, peptides and metal ions into large unilamellar vesicles. *Biochimica et Biophysica Acta*, 1331(2), 187–211.
29. Rasia, M., & Bollini, A. (1998). Red blood cell shape as a function of medium's ionic strength and pH. *Biochimica et Biophysica Acta*, 1372(2), 198–204.
30. Petrov, P. G., & Döbereiner, H. G. (2000). Light-induced shape transitions of giant vesicles. In P. L. Luisi & P. Walde (Eds.), *Giant vesicles* (pp. 336–339). Chichester: Wiley.
31. Nishiguchi, E., Sindo, J., & Hamasaki, N. (1993). Requirement of cytoplasmic components for lidocaine-induced shape change in human erythrocytes. *Biochimica et Biophysica Acta*, 1176(1–2), 95–105.
32. Huang, C.-h., & Li, S. (1999). Calorimetric and molecular mechanics studies of the thermotropic phase behavior of membrane phospholipids. *Biochimica et Biophysica Acta*, 1422(3), 273–307.
33. Hata, T., Matsuki, H., & Kaneshina, S. (2000). Effect of local anesthetics on the bilayer membrane of dipalmitoylphosphatidylcholine: Interdigitation of lipid bilayer and vesicle-micelle transition. *Biophysical Chemistry*, 87(1), 25–36.
34. Takeda, K., et al. (2009). Effect of local anaesthetic lidocaine hydrochloride on the bilayer structure of phospholipids. *Journal of Oleo Science*, 58, 369–377.
35. Matsingou, C., & Demetzos, C. (2007). Calorimetric study on the induction of interdigitated phase in hydrated DPPC bilayers by bioactive labdanes and correlation to their liposome stability: The role of chemical structure. *Chemistry and Physics of Lipids*, 145(1), 45–62.
36. Moraes, C. M. (2007). Preparação e caracterização físico-química de complexos de inclusão entre anestésicos locais e hidróxi propil-β-ciclodextrina. *Química Nova*, 30, 777–784.
37. Barceloux, D. G. (2012). *Medical toxicology of drugs abuse: Synthesized chemicals and psychoactive plants*. Hoboken, NJ: Wiley.
38. Ueda, I., et al. (1994). Local anesthetics destabilize lipid membranes by breaking hydration shell: Infrared and calorimetry studies. *Biochimica et Biophysica Acta*, 1190(2), 421–429.
39. Malheiros, S. V. P., et al. (2004). A new look at the hemolytic effect of local anesthetics, considering their real membrane/water partitioning at pH 7.4. *Biophysical Chemistry*, 110(3), 213–221.
40. Garcia, D. A., & Perillo, M. A. (1997). Supramolecular events modulate flunitrazepam partitioning into natural and model membranes. *Colloids Surfaces B: Biointerfaces*, 9, 49–57.
41. Frye, J., et al. (1985). Cross polarization P-31 nuclear magnetic resonance of phospholipids. *Biophysical Journal*, 48(4), 547–552.
42. Koynova, R., & Caffrey, M. (1998). Phases and phase transitions of the phosphatidylcholines. *Biochimica et Biophysica Acta*, 1376(1), 91–145.
43. Almeida, A. C. P.d. (2008). *Lidocaína lipossomal produzida em processo escalonável: formulação, caracterização e testes biológicos*. Campinas: Universidade Estadual de Campinas.
44. Mitragotri, S., et al. (1999). An analysis of the selectivity of solute partitioning. Diffusion and permeation across lipid bilayer. *Biophysical Journal*, 77, 1268–1283.
45. Fernandes Fraceto, L., et al. (2005). Differential effects of uncharged aminoamide local anesthetics on phospholipid bilayers, as monitored by ¹H-NMR measurements. *Biophysical Chemistry*, 115(1), 11–18.
46. de Verteuil, F., et al. (1981). Phase diagrams for impure lipid systems: Application to lipid/anaesthetic mixtures. *Biochimica et Biophysica Acta*, 640(1), 207–222.
47. Hata, T., et al. (2001). Partition coefficients of charged and uncharged local anesthetics into dipalmitoylphosphatidylcholine bilayer membrane: Estimation from pH dependence on the depression of phase transition temperatures. *Colloids and Surfaces B: Biointerfaces*, 22(1), 77–84.
48. Pasenkiewicz-Gierula, M., et al. (2003). Effects of a carane derivative local anesthetic on a phospholipid bilayer studied by molecular dynamics simulation. *Biophysical Journal*, 85(2), 1248–1258.
49. Lorite, G. S., et al. (2009). Dibucaine effects on structural and elastic properties of lipid bilayers. *Biophysical Chemistry*, 139, 75–83.
50. Fernandez, M. F. (1981). Disruption of liposomes by tetracaine micelles. *Biochimica et Biophysica Acta*, 647, 27–30.
51. Hamill, O. P., & Martinac, B. (2001). Molecular basis for mechanotransduction in living cells. *Physiological Reviews*, 81, 685–740.

52. Inoko, Y., & Mitsui, T. (1978). Structural parameters of di-palmitoyl phosphatidylcholine lamellar phases and bilayer phase transitions. *Journal of Physiological Society of Japan*, 44, 1918–1924.
53. Kodama, M., Kuwabara, M., & Seki, S. (1982). Successive phase-transition phenomena and phase diagram of the phosphatidylcholine–water system as revealed by differential scanning calorimetry. *Biochimica et Biophysica Acta*, 689(3), 567–570.
54. Wildsmith, J. A. W., et al. (1987). Differential nerve-blockade: Esters vs. amides and the influence of pKa. *British Journal of Anaesthetics*, 59, 379–384.
55. Fujii, T., et al. (1979). Shape changes of human erythrocytes induced by various amphipathic drugs acting on the membrane of the intact cells. *Biochemical Pharmacology*, 28, 613–620.
56. Mattila, M. A., et al. (1983). The efficacy and plasma concentrations of flunitrazepam after oral or intramuscular premedication. *International Journal of Clinical, Pharmacology, Therapeutics and Toxicology*, 21, 284–286.
57. Grahnen, A., et al. (1991). Inter- and intraindividual variability in the concentration-effect (sedation) relationship of flunitrazepam. *British Journal of Clinical Pharmacology*, 31, 89–92.
58. de Paula, E., et al. (2012). Micro and nanosystems for delivering local anesthetics. *Expert Opinion on Drug Delivery*, 9, 1505–1524.
59. Rousseau, G. F., et al. (2002). Plasma lidocaine concentrations following insertion of 2% lidocaine gel into the uterine cavity after uterine balloon thermal ablation. *British Journal of Anaesthetics*, 89, 846–848.
60. Atanassoff, P. G., Weiss, B. M., & Brull, S. J. (1996). Lidocaine plasma levels following two techniques of obturator nerve block. *Journal of Clinical Anesthesiology*, 8, 535–539.
61. Merle, J. C., et al. (1999). A comparison of two techniques for cervical plexus blockade: Evaluation of efficacy and systemic toxicity. *Anesthesia and Analgesia*, 89, 1366–1370.